FEATURE ARTICLE

Two-Dimensional Crystallization of Streptavidin Mutants

Szu-Wen Wang, Channing R. Robertson, and Alice P. Gast*

Department of Chemical Engineering Stanford University Stanford, California 94305-5025

Received: February 26, 1999; In Final Form: June 1, 1999

Many applications motivate investigations of the physical factors governing protein assembly in two dimensions, including two-dimensional (2D) protein crystallization for complex structural analyses and the development of technologies such as biosensors and engineered biomaterials. In addition, 2D macromolecular ordering is of fundamental interest in the areas of phase behavior and complex fluids. Our work involves the growth of 2D streptavidin crystals to examine protein self-assembly at an interface. Streptavidin molecules bound to a biotinylated lipid monolayer self-assemble into ordered arrangements, creating 2D crystals with distinct macroscopic morphologies and lattice configurations. In this paper, we highlight previous work examining the effects of intermolecular interactions on molecular organization and macroscopic properties in ordered protein arrays. We also describe our recent progress using streptavidin mutants to study specific protein−protein interactions and their effects on crystal properties. We show that specific changes in intermolecular interactions give alternate morphological, crystallographic, and thermodynamic properties in ordered monolayers. We introduce an additional growth direction in a crystal with oblique *P*1 symmetry by engineering extra hydrogen bonds. These extra interactions kinetically trap the crystal in a less-ordered paracrystalline state; however, a solid−solid phase transition to the more-ordered, thermodynamically favored form occurs over time. Removal of this interaction enables molecules to directly form the more-ordered *P*1 configuration. The introduction of repulsive forces at this site inhibits *P*1-crystal formation such that crystals with *P*2 symmetry grow at conditions normally resulting in *P*1 crystals. Our results confirm that macrosopic and microscopic changes in 2D crystalline properties can be elicited by selectively altering specific intermolecular interactions. Such specific engineered alterations are useful in producing desired crystals and to further our understanding of protein interactions and assembly.

Introduction

The influence of intermolecular interactions on molecular organization and macroscopic properties is an intriguing subject with practical applications beyond the field of statistical mechanics. These types of investigations in systems such as polymer suspensions, colloidal dispersions, microemulsions, and protein solutions are further complicated by the intricate nature of these complex fluids.[1,2] Of particular interest are the ordering and phase transition properties in these systems. Studies of phase transitions and self-assembly in two-dimensional (2D) lipid[3,4] and protein systems[5,6] are key to understanding cell membranes and numerous other biological functions. These include interesting structural changes in the 2D crystals comprising the tail sheath of a bacteriophage during its penetration into a bacterium,[7] mechanisms of lung surfactant lipids and proteins,[8,9] and S-layer proteins coating bacterial cell surfaces.[10,11] Ordered protein monolayers are used for structure determination of proteins recalcitrant to traditional crystallization protocols, consequently elucidating mechanisms for biological function. In addition, they can serve as nucleation sites to epitaxially grow three-dimensional (3D) crystals.[12,13] These studies are relevant to the development of technologies such as biosensors and engineered biomaterials, since such devices often employ and seek to control biological macromolecules at an interface.[14]

An essential element to manipulating ordered self-assembly is to understand the effects of interactions between macromolecules on the physical properties and phase behavior of 2D biomolecular ordering. While these are important fundamental concerns, relatively little is known regarding the mechanisms by which such interactions lead to self-organization. We sought to gain this understanding through studies of the 2D crystallization of streptavidin on a biotinylated lipid monolayer.[15−17] In the work described in this paper, we manipulated specific intermolecular interactions in a 2D protein system via mutagenesis to investigate the effects of these interactions on molecular arrangement, phase transitions, and macroscopic characteristics. To put the objectives of our work into context, we first provide an overview of prior efforts which serve as a basis for our studies.

Two-Dimensional Ordering. The process of self-assembly in two dimensions has been employed to study general aspects of crystallization and phase transitions. Molecules or particles confined to a single monolayer have fewer degrees of freedom than in three dimensions, making experimental analysis and theoretical modeling simpler. In addition, 2D phase transitions are fundamentally intriguing; the solid-to-liquid melting transition is predicted to be continuous in two dimensions and, therefore, is inherently different than the first-order, three-dimensional transition.[18−21] While 2D ordering has been investigated with mesoscopic objects on the millimeter scale[22] and with colloidal particles near micron-sizes,[23−25] most studies involve molecules at angstrom or nanometer scales.

Among the subjects of this last group are amphililic molecules, such as phospholipids.[3,4] These molecules are deposited

* Corresponding author.

10.1021/jp990715s CCC: $18.00
Published on Web 08/18/1999

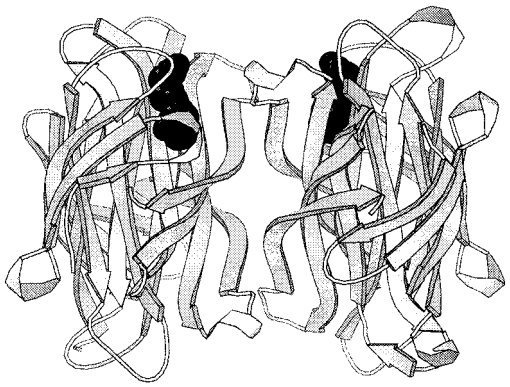

Figure 1. Side-view of the streptavidin molecule. The two black spacefilled molecules are biotin, which are covalently attached to lipid in the monolayer and bound by two streptavidin subunits. The alternate pair of subunits on the opposite face of the protein remain unbound. Figures 1, 4, and 5 were created with the molecular visualization software MOLSCRIPT.[42]

on a Langmuir trough to form a single monolayer at the air−water interface, and phase behavior is studied by monitoring the surface pressure as the area is compressed or expanded.[26] Researchers subsequently discovered that the ordering of proteins in two dimensions can be accomplished by attaching proteins to these phospholipid monolayers. Initial experiments took advantage of specific ligand−receptor interactions to bind these proteins to the monolayer, and among the first proteins to be crystallized in this way were antibodies[27] and cholera toxin.[28] Less specific types of binding, such as electrostatic attractions[29,30] and metal−chelation to surface histidines,[31] have also been successful means to order proteins on a lipid layer. A review of proteins and the various methods used for their 2D crystallization is given in Jap et al.[5]

Two-dimensional protein crystallization is especially advantageous for the determination of protein structure for large protein complexes not amenable to traditional 3D crystallization techniques.[29] Recent examples include DNA and transcription factors bound to RNA polymerase complexes.[32,33] First developed by Henderson and co-workers to solve the structure for bacteriorhodopsin,[34] this method involves obtaining electron micrographs of these crystals and performing Fourier analysis to determine electron density projection maps. It is also possible to obtain a three-dimensional protein structure from micrographs of a 2D crystal taken at different angles of tilt relative to the incident electron beam.

Model Protein System: Streptavidin. In our investigation of 2D protein crystallization, we use streptavidin as a model protein. This protein is well-characterized and exhibits many unusual and useful properties.[35−39] It exists as a tetramer of four identical subunits, totaling a molecular weight of approximately 58 kd.[35,39] These subunits possess a high binding affinity to the vitamin biotin (with $K_D = 10^{-15}$ M),[40] and the overall molecule displays 222 point group symmetry such that its two pairs of biotin binding sites exist on opposite faces of the protein[41] (Figure 1). In addition, it is stable over substantial variations in pH and temperature.[37,40,43] These attributes have made streptavidin and its homologous protein avidin useful in numerous applications, including purification processes and immunoassays.[36] The study of streptavidin monolayer ordering is especially relevant, since many potential applications ranging from biomaterials to biosensors can be envisioned by confining this unique protein to a plane.[44−47]

Weber and co-workers determined the three-dimensional crystal structure of streptavidin to a resolution of 2.6 Å[41] and found that significant conformational changes occur upon biotin-binding by a subunit. More recently, Stenkamp and co-workers[48] determined the structure of streptavidin containing two biotin-bound subunits and two biotin-free subunits (on opposite faces of the molecule), corresponding to the state of streptavidin bound to a biotinylated lipid monolayer (Figure 1). For these reasons, we use this structure (obtained from Brookhaven Protein Data Bank, accession code 1swd) for our molecular models. Knowledge of specific amino acid positions facilitates our studies of the relationship between protein−protein interactions and 2D crystallization and allows us to make systematic point mutations to test our hypotheses.

2D Streptavidin Crystal Morphologies and Molecular Composition. Several studies found that streptavidin is readily crystallized on a biotinylated lipid monolayer in a Langmuir trough[15,16] and that the growth of these crystalline domains can be observed with fluorescence microscopy. Recent work by Leckband demonstrates that similar crystals can be grown directly on lipid layers adsorbed to solid surfaces.[49] The high affinity of streptavidin to biotin ensures that protein interactions and crystallization are limited to two dimensions, simplifying further analyses.

Early studies of 2D streptavidin monolayers noted the curious H-shaped morphologies observed at neutral pH[15] (Figure 2A). Darst and co-workers determined that these crystals consist of an array of molecules arranged in a square lattice (space group *C*222); unit cell parameters are $a = 58$ Å, $b = 58$ Å, and $\gamma = 90°$ for a unit cell containing one molecule.[12,16] Subsequently, our studies reported a variability in crystal morphologies at pH = 7, ranging from H- to dendritic-X shapes.[17,50] We found that these morphologies vary with the amount of streptavidin impurities present in the protein preparation and that these impurities cause a dendritic growth instability due to transport limitations reminiscent of Mullins−Sekerka growth[51] (Figure 2B). Addition of avidin, a noncrystallizable protein homologous to streptavidin, to preparations of homogeneous streptavidin reproduces these dendrites. As the streptavidin/avidin ratios and concentrations are changed, different dendritic morphologies result, including secondary branching and coarsening. In accord with the Mullins−Sekerka model, we showed that growth rate of the dendrites increases linearly with the concentration of streptavidin and is roughly inversely proportional to the square of the tip radius of curvature.[50,51] Observations of crystalline streptavidin domains improve by the addition of avidin, which separates individual streptavidin crystals and provides a background for fluorescence contrast.

The effects of differences in the protein−protein interactions are observed in these crystals. The rectangular shape of early *C*222 crystals at neutral pH and of *C*222 crystals grown at pH > 8 show two major growth directions; aspect ratios indicate that the length grows approximately 2−3 times faster than the width.[50,52] From experimental results[53] and theoretical calculations,[50,54] we predicted that the observation of a preferred growth direction can be attributed to the differences in the intermolecular contacts between the biotin-bound monomers and the unfilled monomers of each streptavidin tetramer. Subsequent work by Vogel and co-workers supported this; they observed that binding of streptavidin to a monolayer of copper-chelated lipid through coordination with surface histidines (leaving all subunits biotin-free) yields square crystals.[31,55]

Since the natural environment of proteins is aqueous, the protein surfaces contain numerous hydrophilic groups, including charged side chains. Therefore, one anticipates many opportunities for electrostatic and hydrogen-bonding interactions between

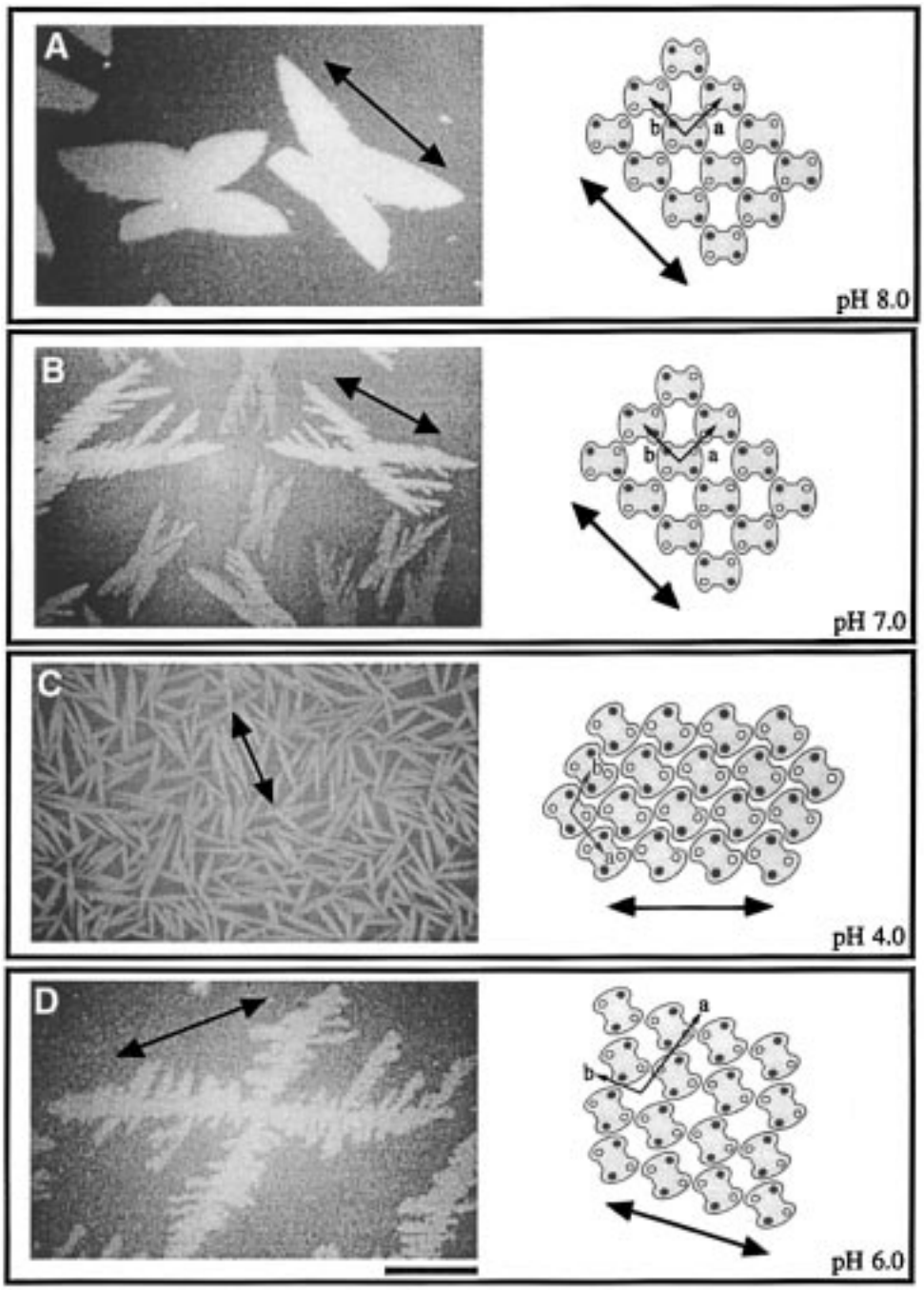

Figure 2. Morphologies and molecular arrangements at pH = 7−8, pH = 6, and pH = 4. Arrows indicate preferred growth directions. In crystal lattice drawings, (a) and (b) refer to crystal lattice parameters and are scaled accordingly.[60] Closed and open circles refer to biotin-bound and biotin-free subunits, respectively. (Scale bar = 100 μm.) (A) H-shaped domains with *C*222 symmetry grown in the absence of avidin at pH = 8. The molecular arrangement for the *C*222-crystal form is shown. The preferred growth direction is along the biotin-bound subunits. (B) Dendritic-X domains with *C*222 symmetry grown with avidin at pH = 7. The molecular arrangement and preferred growth direction is the same as in part A. (C) Needle-like domains with *P*1 symmetry grown at pH = 4. The molecular arrangement for the *P*1-crystal form is shown. The preferred growth direction has both biotin-free and biotin-bound subunits in contact. (D) Dendritic-X domain with *P*2 symmetry grown with avidin at pH = 6. The molecular arrangement for the *P*2-crystal form is shown. The preferred growth direction is along the biotin-free subunits.

adjacent proteins packed into a crystal lattice and that changing these functional groups affects molecular configuration. Indeed, many examples exist in the literature showing that pH changes result in crystals with different packing geometries.[56,57]

In the ordered 2D streptavidin system, microscopic lattice differences are evident in the macroscopic morphologies. Investigations by Hemming et al.[12] show that molecules in 2D streptavidin crystals grown at pH = 4 give a more compact arrangement with unit cell parameters of $a = 58$ Å, $b = 50$ Å, and $\gamma = 113°$, corresponding to the *P*1 space group. This form grows into needle-like domains[52] (Figure 2C). We identified a third 2D crystal type existing between pH ∼ 5.5−6.[58] This crystal shows *P*2 symmetry,[59] with the average unit cell parameters $a = 116 \pm 1$ Å, $b = 58 \pm 0.4$ Å, and $\gamma = 107 \pm 1°$ and corresponds to dendritic-X morphologies similar to those observed at pH = 7 (Figure 2D).[60]

We found that transitional variations of several different crystal morphologies exist in the intermediate pH range of 4.5−7. Between pH = 4.5−5.7, these include chiral inverse-S-domains (Figure 3A), wide-needle structures (Figure 3B), and

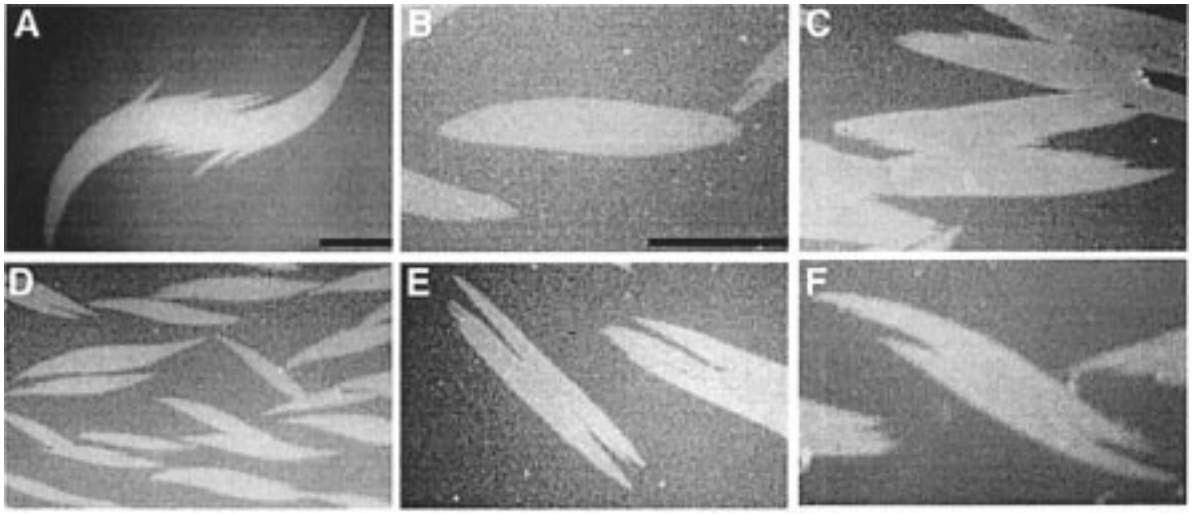

Figure 3. Intermediate morphologies seen at pH = 5−5.7. These crystal domains consist of different ratios of coexisting *P*1, *P*2, and *C*222 crystals. (Scale bars = 100 μm; scale for parts B−F is the same.) (A) Chiral inverse-S-domain. (B) Wide-needle domain. (C) H-shaped domain. (D) Needle-like domains with chiral characteristics. (D) Wide-needle domain with split ends. (E) Inverse-S-domain with split ends.

H-domains (Figure 3C). We also obtained morphologies intermediate to these geometries, such as needle-like domains with chiral ends (Figure 3D), wide-needle domains with split ends (Figure 3E), and inverse-S-domains with split ends (Figure 3F). While we observed only three 2D streptavidin crystals (*P*1, *P*2, *C*222), the large variety of unusual and intermediate morphologies results from the different coexisting ratios of these three crystals within each domain.[60] At pH $\sim$ 5.7−7, crystals give dendritic-X morphologies reminiscent of those seen at pH = 7 (Figure 1B,D). Despite the similarity in domain shapes at this pH range, morphologies consist of varying amounts of coexisting *P*2 and *C*222, with 100% *P*2 near pH = 5.7, 100% *C*222 near pH = 7, and intermediate *P*2/*C*222 ratios at intermediate pH values. In all cases, the observations of coexistence imply that energetic differences between coexisting crystals are small, which is supported by the observation of coexistence near the reported isoelectric point (pH = 5−6).[37,38]

These domains show varying degrees of growth anisotropy, and with molecular packing information, the identification of important interactions is possible. We therefore determined the 2D molecular arrangement of the three crystal forms and coexisting crystals relative to their macroscopic morphology.[60] We found that, in the *C*222-crystal form, differences in interactions between the biotin-bound and biotin-free subunits of adjacent streptavidin molecules result in faster growth along the biotin-bound direction. In the *P*2-crystal form, the opposite is true; the preferred growth direction is parallel to the direction of the biotin-free subunits. *P*1 crystals, being significantly more compact than either *P*2 or *C*222 crystals, exhibit strong growth anisotropy corresponding to interactions between both biotin-bound and biotin-free subunits. These characteristics apply in domains which are entirely *P*1, *P*2, or *C*222 and in domains with coexisting crystals.

Changes in Interactions via Mutagenesis. These investigations show that pH changes result in significant alterations in macroscopic morphologies and microscopic arrangement.[16,52,57] Therefore, the ability to finely control and direct electrostatic interactions is a key factor to controlling the lattice structure, and consequently the properties, of protein arrays. While pH-change investigations are useful, one limitation is their lack of specificity in targeting certain interactions for further study. As a complement to our previous studies, therefore, we also used site-directed mutagenesis for altering specific interactions.

Examples exist using mutagenesis at crystal contacts to improve 3D crystal quality for X-ray diffraction analysis.[61−64] Protein mutants also exhibit different crystallization properties in two dimensions. For example, apoferrin mutants yield 2D crystals with different symmetries; unlike the streptavidin system, however, these proteins are not specifically bound to the monolayer and can sample many other configurations.[65] Recent work in the 2D streptavidin system[66] shows that mutagenesis of a lysine to leucine at a *C*222 contact site enables *C*222 crystals to grow in the absence of salt in the subphase. In addition, we found that the presence of three extra amino acids at the C-terminal end of the "core" streptavidin molecule inhibits *P*1 formation through steric means.[67]

To localize interaction modifications, we changed a single amino acid at a specific crystal contact in the low-pH-crystal form to enhance and to suppress attractive and repulsive forces. From these results, we gain a better understanding of the extent to which a specific interaction alters crystal formation and changes crystalline physical properties. In this section, we discuss the results and implications of changes at a particular interaction site in the *P*1 crystal.

Materials and Methods

Molecular Modeling. Three-dimensional crystal coordinates for streptavidin molecules are available from the Protein Data Bank (PDB, Brookhaven National Laboratory). We use the structure reported by Freitag et al. (PDB accession code 1swd),[48] which best represents the streptavidin in our 2D monolayer system, since one pair of monomers binds to the lipid monolayer while the other pair faces the subphase and remains unbound. Molecules were manually docked in *C*222, *P*1 (Figure 4), and *P*2 unit cell configurations according to lattice cell parameters[12,16,58] and molecular orientation relative to biotin binding.[60] Regions of interest were identified using Biosym (InsightII) and Rasmol. Our results (discussed in the Results and Discussion section) show that aspartate 36 (Asp36), which is at a *P*1-crystal contact, is a good site for altering interactions. We mutated this position to alanine (D36A), asparagine (D36N), and lysine (D36K) (Table 1) for reasons discussed below.

Mutagenesis and Protein Expression. We obtained streptavidin genes encoding wild-type amino acids and spanning residues 13−139 and 13−136 from Professor Patrick Stayton

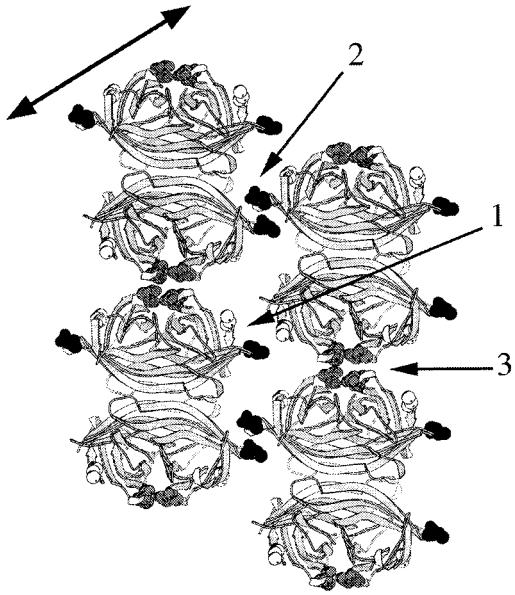

Figure 4. Carbon-chain backbone representation of four streptavidin molecules in *P*1 arrangement (top view). Crystal coordinates are available only for amino acids 16−133 for three monomers in each tetramer (and 16−132 for the fourth monomer).[48] Light-gray spacefilled molecules are the first residue at the N-terminal end (amino acid 16), dark-gray space-filled molecules are the last residue at the C-terminal end (amino acid 133), and medium-gray spacefilled molecules is residue 36. The heavy line with two arrowhead represents the preferred growth direction in wild-type streptavidin.[60] **1**, **2**, and **3** are the three contact regions in the *P*1 crystal. Biotin molecules (not shown) are bound in the top right and bottom left subunits of each streptavidin molecule.

TABLE 1: Amino Acid Side Chains in Mutagenesis[a]

amino acid 36	side chain
wild-type	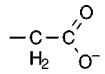
D36N	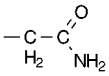
D36A	
D36K	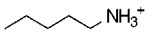

[a] Wild-type (aspartate); D36N, asparagine; D36A, alanine; D36K, lysine.

(University of Washington).[68] Streptavidin produced naturally by *Streptomyces avidinii* undergoes posttranslational processing, resulting in many different protein lengths ranging from amino acid ∼13−14 to ∼133−139.[41,69,70] In previous work, we found that streptavidin 13−139 does not form *P*1 crystals at low pH due to steric hindrance caused by residues 137−139 and that removal of these C-terminal amino acids allows formation of *P*1 crystals.[67] Therefore, we created Asp36 mutants using the DNA template for the 13−136 form in these experiments.

Complete details of the mutagenesis and protein expression protocols are provided in reference 71. We performed point mutations by cassette mutagenesis. Four custom oligonucleotides were made: three reverse primers encoding for the three different Asp36 mutants and one forward primer. Mixtures of each primer set were annealed, extended, and cloned into the 13−139 gene contained in a pUC18 plasmid. Plasmids containing mutated Asp36 positions were selected and the streptavidin mutants were sequenced. Since the 13−139 protein form could not be used to study *P*1 crystals, the region of each mutant gene containing the respective mutated Asp 36 was cloned into a 13−136 streptavidin gene contained in expression vector pET21a. The streptavidin genes were again sequenced to confirm DNA sequences before transformation into the expression host, BL21(DE3) *E. coli* cells.

Expression and purification were accomplished following the protocol reported in previous streptavidin studies.[66,68,72] Cells were grown, induced with isopropyl-β-D-thiogalactopyranoside, harvested, and lysed. Inclusion bodies were washed, solubilized, and refolded. Proteins were purified on an iminobiotin column as described in Hofmann et al.[43] Analysis with MALDI-TOF mass spectrometry gave molecular weight peaks of 13 003, 13 046, and 13 064 for D36A, D36N, and D36K monomers, respectively, which were all close to predicted mass (within accuracy for the technique). These values, together with DNA sequence results, confirmed the presence of purified mutants of the appropriate length and mutation.

2D Crystallization. Two-dimensional crystallization of mutant streptavidin was performed in a Langmuir trough as described previously.[17,50] A miniature Langmuir trough (8.5 mm × 37 mm × 4 mm) was filled with buffer containing 50 mM NaH_2PO_4 and 500 mM NaCl in Milli-Q filtered water with the pH adjusted using NaOH. The buffer was again filtered with a 0.2 μm filter before addition into the trough. A lipid mixture consisting of 0.015 mg/mL *N*-((6-(biotinoyl)amino)hexanoyl)-1,2-dihexadecanoyl-*sn*-glycero-3-phosphoethanolamine and 0.15 mg/mL dioleoylphosphatidylcholine in 1:1 chloroform/hexane was spread on the aqueous subphase and compressed to a surface pressure of approximately 25 mN/m.

A 1:1 molar mixture of nonlabeled (mutant) streptavidin and fluorescently labeled, noncrystallizable avidin was injected beneath the trough barrier into the aqueous buffer to give a bulk protein concentration of approximately 200 nM. Crystallization spontaneously occurred at room temperature and morphologies of streptavidin crystals were observed with a Zeiss Axioplan epifluorescence microscope. We fluorescently labeled avidin using the protocol described by Nargessi and Smith.[73] This provides visual contrast and dilutes our mutant protein, giving better separation and observation of individual streptavidin domains. While avidin is homologous to streptavidin and has similar binding characteristics to biotin,[37,39] it does not crystallize in this 2D system[17] because it is heterogeneously glycolysated.[74] In previous work we show that addition of avidin does not affect the crystal packing structure of streptavidin crystals.[58]

For some experiments, crystals were observed over a time period of 1−3 days. During this time, the trough and crystals were kept in a hydrated container to prevent subphase evaporation. After each experiment, pH values were assessed and found to remain constant over the course of the experiment, indicating that any changes observed in crystal morphology or crystal form were not due to changes in pH.

Electron Microscopy and Diffraction Analysis. In the preparation of samples for transmission electron microscopy (TEM), cross-linking of crystals was necessary to ensure stability during transfer. Glutaraldehyde was gently injected into the buffer subphase to a final concentration of 0.5%. Diffusion through the buffer and reaction with protein was continued for at least 4 h. We found that treating the crystals in this way does not change lattice parameters within the resolution discussed here.[53] Copper−rhodium TEM finder grids were coated with a thin layer of carbon using the standard method outlined in ref 75, and transfer of crystals was accomplished as described in a previous paper.[58] Grids were washed briefly with water and negatively stained with 1% uranyl acetate. Samples were

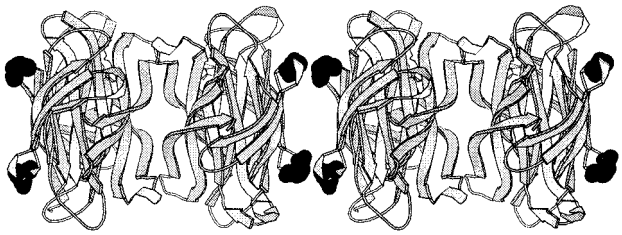

Figure 5. Side view of two adjacent streptavidin molecules showing contact 3 in the *P*1-crystal form. Biotin molecules (not shown) are bound in the top monomers, and Asp36 residues are highlighted.

observed with a TEM (Philips TEM400) and micrographs were taken of crystals at a magnification of 36000×. Diffraction analysis was conducted using an optical diffractometer, and previously described digitization and computation protocols.[16,34,76] Because of the large number of data (from the different mutants at different pH values), not all the diffraction patterns are reported here; diffraction published in our previous studies[58,60] are representative of those we observed in this work.

Molecular Modeling of Potential *P*1 Interactions. We are interested in the interactions contributing to the formation of crystals with *P*1 symmetry.[12] Three main contact regions occur in the *P*1-crystal form: one contact along the preferred growth direction (contact 1 in Figure 4), one between C-terminal ends (contact 2 in Figure 4), and another along the "length" of the molecules (contact 3 in Figure 4). Since the *P*1-crystal form appears at low pH values, we identified those surface amino acids which would change electrostatic character in this pH range; these are glutamates and aspartates, which have respective side-chain pK_a ranges of 4.3−4.5 and 3.9−4.0.[77] Contact regions 1 and 2 contain both the C-terminal and N-terminal ends of streptavidin, which unfortunately have not been resolved in the 3D protein structure used to model our monolayer system.[48] This indicates that the ends are flexible and poorly ordered, and may not be good areas for the study of intermolecular interactions. Since we cannot accurately model the specific intermolecular protein interactions involved in crystallization for contact regions 1 and 2, we focused on the third contact region for our mutagenesis experiments.

We determined that, in contact region 3, the only ionizing amino acid at low pH is aspartate 36 (Asp36), and it appears to be a key participant in *P*1 crystal formation (Figure 5). In the *P*1 configuration, the side chains of Asp36 are directed toward each other and within the distance for potential electrostatic interactions (Debye length ≈ 4 Å at this ionic strength) and hydrogen bonding. We reasoned that, at pH = 4, statistically half these positions are protonated and neutral, and the other half are negatively charged, allowing for an average of one potential hydrogen bond per aspartate−aspartate contact if side chains are optimally positioned. At high pH values, all aspartates are negatively charged, leading to electrostatic repulsion. This is in accord with the existence of *P*1 crystals only at low pH values. Therefore, we decided to make streptavidin mutants which change the electrostatic character at amino acid position 36 (Table 1). A change to alanine (D36A) removes any potential electrostatic interactions or hydrogen-bonding interactions. An asparagine mutant (D36N) increases the attraction by additional hydrogen bonds at that contact region, and a lysine mutant (D36K) introduces repulsive interactions by electrostatically and sterically disfavoring the formation of *P*1.

Wild-Type Streptavidin Control at pH = 4, 5.25, 7.5. Our previous investigations involving pH changes were performed with commercial streptavidin spanning amino acids 14−136.[55,60,71] However, attempts to produce 14−136 by recombinant means were unsuccessful, due to the failure of N-terminal methionine cleavage.[67] Therefore, in these investigations, we use recombinant streptavidin spanning wild-type amino acids 13−136. Like the commercial streptavidin, this protein produces needle-like crystals at pH = 4 (Figure 6A) consisting of molecules arranged in *P*1 symmetry. Anisotropic growth of *P*1 needles follows the configuration described in Figure 4.

Crystallization behavior is slightly different for this streptavidin form (13−136) than for commercial streptavidin (14−136), and we discuss these differences in reference 67. We find that for streptavidin 13−136 at pH = 5.25, dendritic-X, *P*2 crystals initially form; however, over time, small *P*1 needles emerge from these *P*2 domains, and after 2 days all *P*2 crystals completely convert to *P*1 needles (Figure 7A). (The quality of *P*1 crystal order is discussed later.) At pH = 7.5, the wild-type forms stable dendritic-X crystals with *P*2 symmetry (Figure 6A). Previous experiments also show that streptavidin 13−136 forms *C*222 at pH = 8.8. Although minor differences in crystallization exist between commercial streptavidin (14−136) and recombinant 13−136,[64,68] the important aspect for our experiments described here is the observation of *P*1 crystals with needle-like morphologies for both streptavidin forms at low pH. We found that all three Asp36 mutants display different behavior from the wild-type control at pH = 4; results are summarized in Figure 6 and explained in the following sections.

Two Types of *P*1 Arrangement: Crystal and Paracrystal. When amino acid 36 is mutated from aspartate to asparagine, the extra attractive interactions predicted in contact 3 of Figures 4 and 5 are revealed by a different morphology (Figure 6B). Instead of needle-like crystals, dendritic-X domains are seen resembling morphologies seen at higher pH values. Most interesting in this case are the observations that adjacent arms of the crystals have different lengths, and domains consist of molecules packed in *P*1 symmetry (rather than *P*2 or *C*222). In addition, D36N crystals show time-dependent changes; these dendritic domains change into needles over the course of a few days (Figure 7B), and TEM analysis reveals that these needles are also *P*1 crystals (Figure 8).

From this experiment, we find two types of *P*1 crystals. Solids in the intermediate state between amorphous and crystalline but containing a certain amount of crystallographic order are termed "paracrystals". Many materials are known to exist in this state, including polymers, metals, and proteins.[78,79] We believe that the first type of *P*1 crystal ($P1_p$), seen in D36N domains at pH = 4, has characteristics of this category of materials. The second type ($P1_c$) is more ordered and shows higher quality in one crystallographic direction. This type is observed as the final crystal form for both D36N crystals at pH = 4 and wild-type (13−136) crystals at pH = 5.25 (Figure 7).

Electron microscopy images and diffraction for both these forms of crystals are presented in Figure 8. A comparison of the diffraction patterns shows that reflection (2,−1) is much stronger in $P1_c$ than in $P1_p$, while reflection (1,0) is more evident in $P1_p$. This indicates that $P1_p$ shows a more isotropic quality between the different crystallographic directions and that $P1_c$ crystals have higher crystal quality in one direction. In addition, reflections for $P1_p$ crystals generally tend to be more diffuse and of lower amplitude, indicating less order compared to $P1_c$ crystals. $P1_c$ crystals are also accompanied by line defects in the preferred growth direction[60] and appear in coexistence with *P*2-like domains similar to those described previously.[58] Indeed, rows of molecules are more evident in the preferred growth direction (denoted by "P" in Figure 8C) in images of $P1_c$ than in $P1_p$, and line defects and coexisting *P*2 domains run parallel

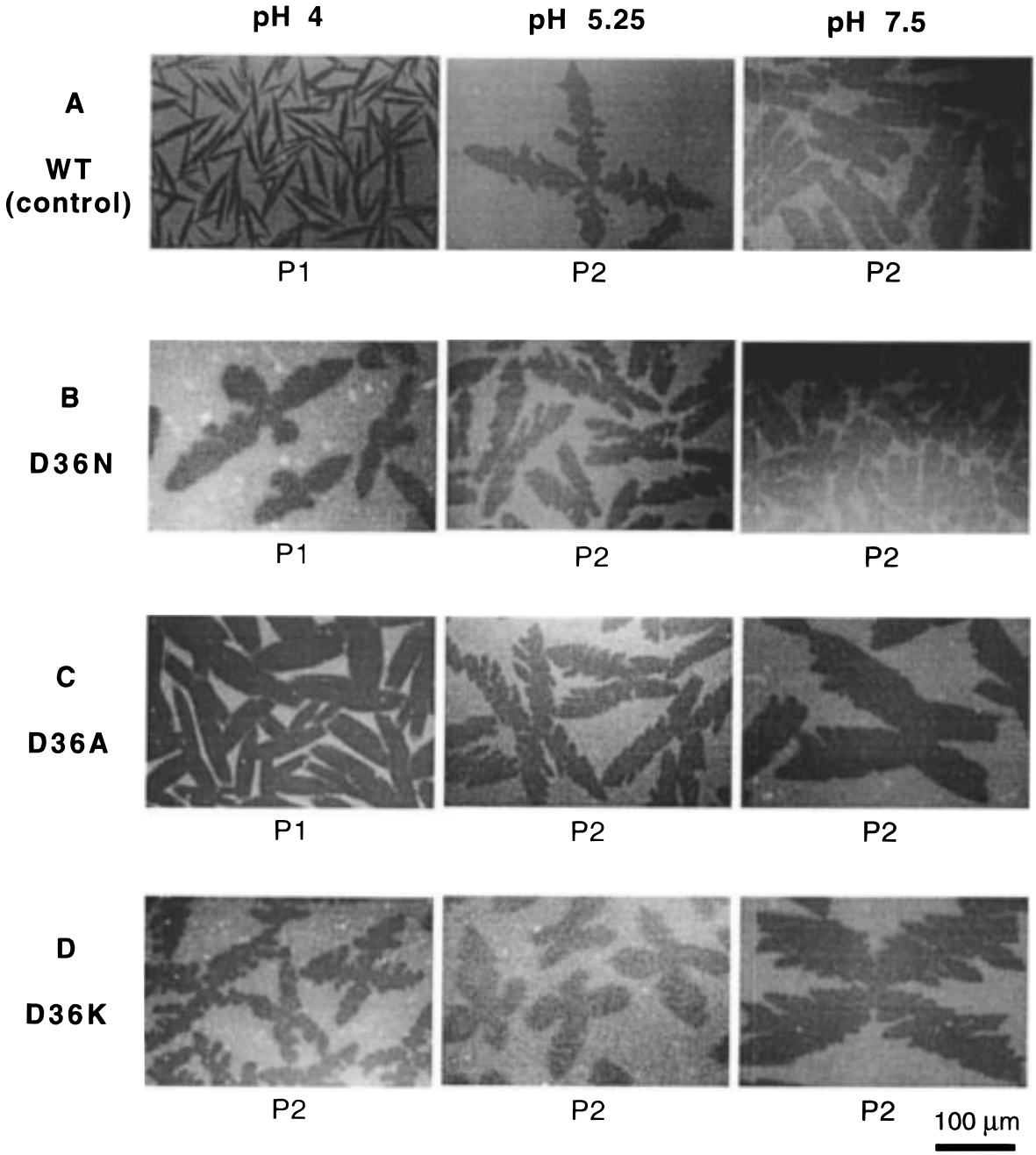

Figure 6. Initial morphologies and crystal forms of mutants at pH = 4, 5.25, and 7.5. Similar to the wild-type control, crystallization of all three mutants at pH = 5.25 and pH = 7.5 gave dendritic-X domains with *P*2 symmetry. (A) Crystals of the wild-type streptavidin control (Asp36) show needle-like domains with *P*1 symmetry at pH = 4. (B) Crystals of the asparagine mutant show anisotropic dendritic-X domains with *P*1 symmetry at pH = 4. (C) Crystals of the alanine mutant show wide-needle domains with *P*1 symmetry at pH = 4. (D) Crystals of the lysine mutant show dendritic-X domains with *P*2 symmetry at pH = 4.

to this direction. A similar phase change has been reported in a study by Gabriel et al.[80] where a transition from a less-ordered to a more-ordered crystal phase for three-dimensional crystals of the annexin protein p68 was observed. Both $P1_p$ and $P1_c$ crystals appear in wild-type needle-like streptavidin domains at pH = 4.

The D36A streptavidin mutant produced crystals having broader needle-like domains (Figure 6). We observed H's and wide needles, similar in morphology to wild-type crystals reported at higher pH values,[60] and TEM analysis revealed that these were $P1_c$ crystals. Unlike the D36N mutant, neither overall crystal morphology nor molecular arrangement changes over the time scale of 1 day. We believe that we have removed significant interactions between the amino acids at position 36 because the alanine side chain does not form electrostatic or hydrogen bonds, and the increased distance between these side chain methyl groups (~7−8 Å) precludes hydrophobic or van der Waals interactions. Removal of this interaction yields crystals exhibiting more order. These data, together with the results from the D36N mutant at pH = 4, suggest that attractive interactions between amino acid 36 result in more overall isotropic ordering in the crystal, and initially kinetically traps the molecules in a $P1_p$ configuration. Geometric constraints in this paracrystal configuration may initially prevent molecules from attaining the higher order seen in $P1_c$ crystals. Removal of this interaction, as in the D36A mutant, allows the molecules to form the more-ordered thermodynamically preferred crystal phase from the outset.

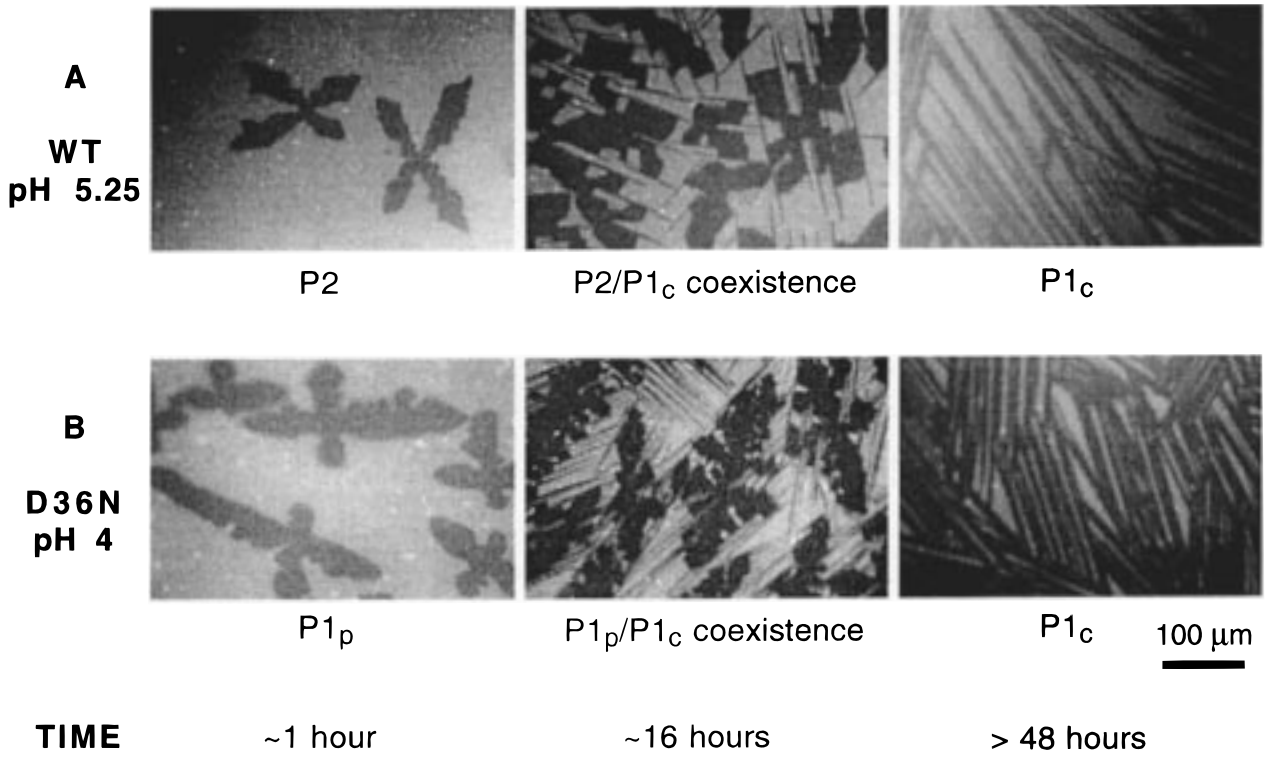

Figure 7. Time-dependent solid−solid-phase transition. $P1_p$ is the less-ordered paracrystalline $P1$ form; $P1_c$ is the more-ordered $P1$ form. (A) Wild-type streptavidin (13−136) changes from dendritic-X crystals ($P2$ symmetry) to needle-like crystals ($P1_c$ symmetry). (B) D36N mutant changes from anisotropic dendritic-X crystals ($P1_p$ symmetry) to needle-like crystals ($P1_c$ symmetry).

New Morphology at pH = 4. The morphology of the crystal domains for the D36N mutant at pH = 4 illustrates the combination of kinetic and transport properties. Dendritic features of the domains are indicative of diffusion-limited growth, while the unusual new crystal morphology results from an enhanced growth rate caused by the introduction of stronger attractive interactions in a direction skewed from the preferred growth direction. Geometric analysis of the $P1$ arrangement predicts an angle of 50.1° between the "original" wild-type preferred growth direction and the direction predicted to form extra hydrogen-bonding interactions (Figure 9). Isolated crystal domains formed within 1−2 h after protein injection give an experimental value of 50 ± 12° (from a data set of 25). This average agrees well with the predicted value and further supports the assessment of the $P1$-preferred growth direction in our previous work[60] and in Figure 4. In addition, the orientation of $P1_c$ needles growing from bulk $P1_p$ D36N domains (Figure 7) also corresponds to the preferred growth direction (P) in Figure 9, further confirming our model.

Time-Dependent 2D Solid−Solid Phase Transition. We observe two types of slow crystalline phase changes in our 2D streptavidin system as described in Figure 7: $P2$ to $P1_c$ for wild-type crystals at pH = 5.25, and $P1_p$ to $P1_c$ for D36N crystals at low pH. We measured initial and final pH values and found no change in pH as the phase changes occurred. This type of time-dependent transformation indicates that the original crystal is a kinetic form and is metastable, and the driving force toward the phase change is the minimization of the thermodynamic free energy. In both transitions, the more ordered $P1_c$ phase is the final result, indicating that $P2$ and $P1_p$ are both metastable phases and that $P1_c$ is the more thermodynamically stable form at the given pH conditions.

Three-dimensional crystalline phase changes are seen in many systems, and often occur following changes in growth conditions, such as pH,[56,57] impurities,[81] and temperature.[82] In addition, morphology and crystalline phase changes without added environmental changes are also observed.[82,83] In the highly studied lysozyme system, Tanaka et al.[83,84] find that changes in salt concentrations produce either spherulitic needle-like crystals or orthorhombic rectangular crystals. At this boundary, crystals are initially needle-like. Over time, they coexist with rectangular crystals until they all convert to the orthorhombic form.

Solid−solid phase changes are attributed to two types of mechanisms: internal rearrangement of molecules nucleating at defects,[85,86] and solvent-mediated phase changes in which the molecules of one crystal form is first dissolved and independently forms elsewhere in the solvent.[87] In our $P2$ to $P1_c$ and $P1_p$ to $P1_c$ phase changes, we are able to examine growth of $P1_c$ within the initial bulk $P2$ or $P1_p$ crystals by observing changes over time with TEM. These observations indicate that our transition occurs through the first mechanism.

Inhibition of *P*1 Crystal Growth. Changing Asp36 to lysine inhibits formation of $P1$ crystals. Dendritic-X crystals with $P2$ symmetry grow at pH = 4 (Figure 6D), and the growth of these domains appears to be significantly slower than wild-type $P2$ crystals at pH = 5.2, the wild-type $P1$ crystal at pH = 4, or the other crystals grown from mutant proteins at pH = 4. Inhibition of $P1$ crystal growth is expected since mutating the 36-position to lysine places two positive larger side chains next to one another, which is both electrostatically and sterically unfavorable. The slower growth of $P2$ crystals suggests that the mutation also may slightly disfavor the $P2$-crystal form (relative to wild-type), possibly because the positive charges of the lysines are placed close to the positively charged amino-terminal group (as seen in molecular modeling). However, the amino-terminal end has not been resolved in the 3D structure,[48] making identification of this interaction speculative. This lack of structure data also shows that the N-terminal end is flexible and can sample many different conformations; therefore $P2$ can still form due to an

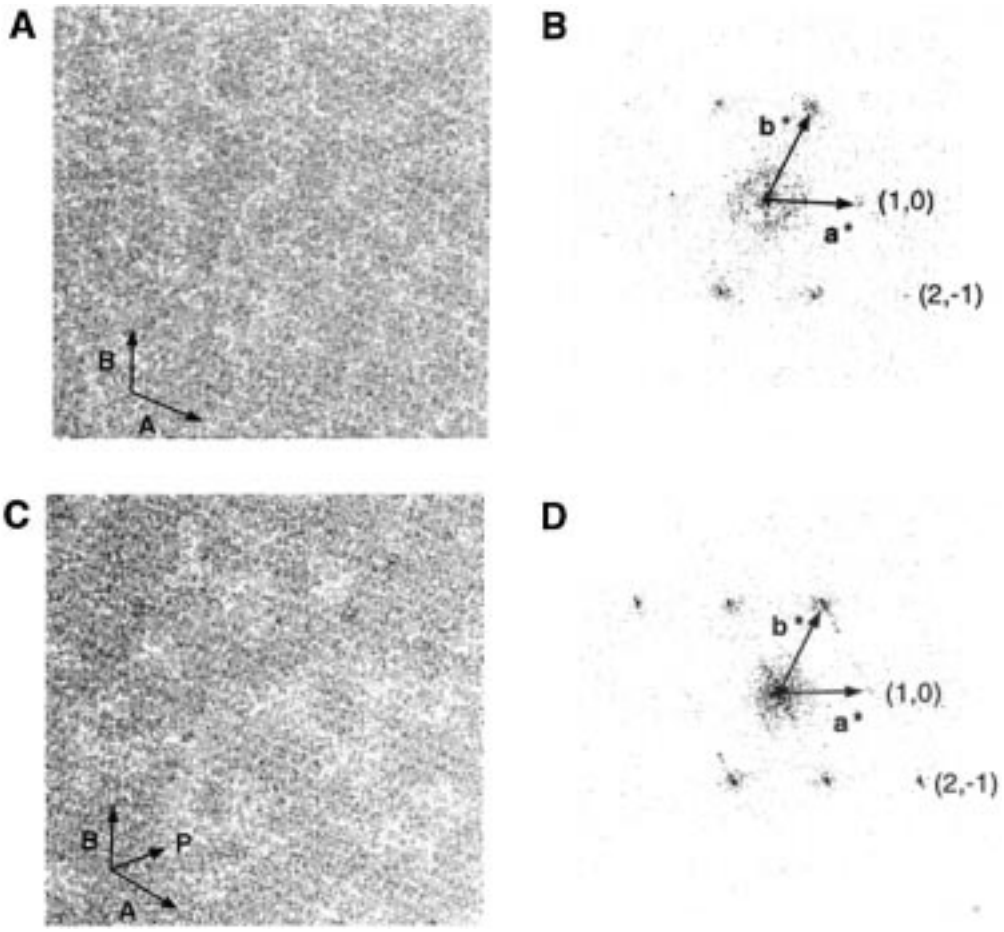

Figure 8. *P*1 crystals and paracrystals. **A** and **B** are lattice cell vectors, and **a*** and **b*** are reciprocal lattice cell vectors. (A) Electron micrograph image of D36N crystals ($P1_p$) at early times. (B) Diffraction pattern for area in part A gives *P*1 crystals with more isotropic crystal quality between the different crystallographic directions. (C) Electron micrograph image of D36N crystals ($P1_c$) after phase transition. **P** is the preferred growth direction. (D) Diffraction pattern for area in part C gives *P*1 crystals with better crystal quality in one crystallographic direction.

alternative placement of the N-terminal amino charge but will grow more slowly. While D36K crystals remain 100% *P*2 over time at pH = 4, the morphology of the crystals change in a way similar to the coarsening effects observed by Ku et al.[17,50] Numerous small, rectangular crystals replace the large dendritic crystals, suggesting that there is a thermodynamic driving force for line tension minimization.

***P*2 Stability at pH = 5.25.** As previously mentioned, we find that at pH = 5.25, wild-type streptavidin (13−136) forms dendritic-X morphologies consisting of molecules arranged in a *P*2 configuration, which rearrange to form $P1_c$ needles over time. We find that while all our mutants also initially form dendritic-X, *P*2 domains at pH = 5.25, only the alanine mutant converts to $P1_c$ needles, but at a much longer time scale than wild-type streptavidin. D36N and D36K crystals both remain dendritic-X and entirely *P*2 in symmetry over the course of 1 day, in contrast with the wild-type control. These observations suggest that changing aspartate to uncharged species such as asparagine and alanine at position 36 destabilizes *P*1 or stabilizes *P*2 at this pH. Since experiments at low pH point to the thermodynamic stability of *P*1 for both D36A and D36N, and the side-chain characteristics of these two amino acids are not expected to change much over this pH range, it is therefore more likely that the mutations stabilize *P*2 (relative to the wild-type). These changes, then, appear to have made a metastable crystal form (*P*2) more thermodynamically stable. The molecular basis of this increased *P*2 stability remains speculative; in the *P*2 crystal, residue 36 appears likely to interact with the N-terminal amino acids 13−15, which unfortunately are also unresolved in the crystal structure.

Crystal Growth at pH = 7.5. As we have previously mentioned, wild-type streptavidin (13−136) forms ∼100% *P*2, dendritic-X domains pH = 7.5. Similar to this control, D36N, D36A, and D36K also give dendritic-X morphologies with 100% *P*2 symmetry at pH = 7.5. This analogous behavior at pH = 7.5 is not surprising. Since these mutations were chosen to alter crystal characteristics at low pH and found also to stabilize the *P*2 crystal at pH = 5.25 relative to wild-type, we would not expect the mutations to result in an alternate crystal form at high pH.

Summary

We find 2D streptavidin crystallization to be a useful model system for fundamental studies of intermolecular interactions in self-ordering protein monolayers. Experiments with pH changes to modify global electrostatic interactions give three different crystals at various pH values (*P*1, *P*2, and *C*222) and several observations unique to the field of ordered protein arrays, including solid-phase coexistence, chiral morphologies, and in situ solid−solid phase transitions. While pH change proves to be a useful method in our studies, one limitation is the global nature of the changes in electrostatic charge distribution. To investigate the effects of specific interaction changes, we modified the streptavidin molecule via genetic manipulation. For these studies, we focused on altering interactions in the *P*1-

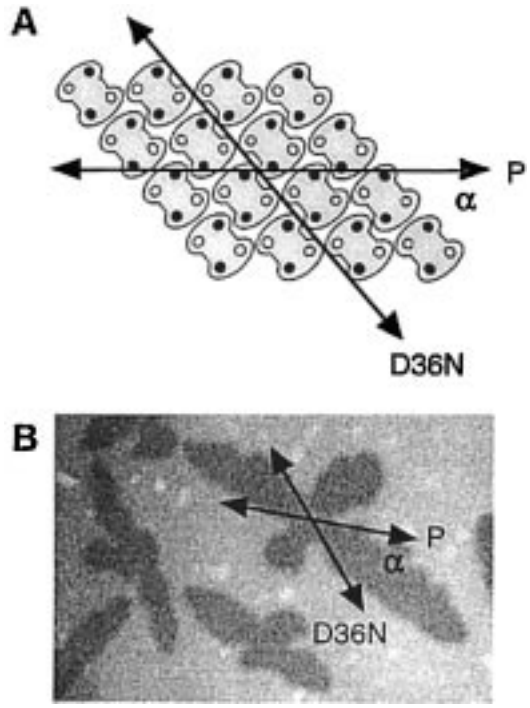

Figure 9. Geometric analysis of crystal morphologies for D36N at pH = 4. **P**, preferred growth direction (of wild-type streptavidin). **D36N**, alternate growth direction introduced by increased number of hydrogen-bond interactions in asparagine mutant. α, angle between **P** and **D36N** growth directions. (A) Theoretically predicted angle between preferred growth direction and new growth direction seen in the D36N mutant is 50.1°. (B) Experimentally determined angle between preferred growth direction and new growth direction is 50 ± 12°. This image has been inverted from the image in Figure 6A such that this domain and the molecules from the model in part A are viewed from the same orientation relative to the lipid monolayer.

crystal form. We find that we can elicit macroscopic and microscopic changes in 2D crystalline properties by selectively altering only one specific intermolecular interaction.

We change the electrostatic characteristics of a *P*1-crystal interaction site involving amino acid 36 by engineering attractive and repulsive interactions between molecules. We observe an additional growth direction in the *P*1-crystal domain by introducing extra hydrogen-bonding interactions. However, these extra interactions kinetically trap the *P*1 crystal in a paracrystalline state, and over time, the thermodynamically preferred, more-ordered *P*1-crystal forms via a solid−solid phase transition. Removal of interactions between the adjacent side chains of amino acid 36 allows the molecules to directly form the more-ordered *P*1 configuration. Introduction of repulsive forces at this interaction site inhibits *P*1-crystal formation, resulting in *P*2 crystals at low pH. Therefore, in these specific interaction modifications, we alter crystal characteristics including morphology, crystal quality, crystal phases, and kinetic and thermodynamic behavior.

These experiments introduce several opportunities for further investigations. Our results show that mutagenesis can be used to determine important crystallization interactions and to modify various crystalline properties. Other investigations are envisioned involving the residue 36 interaction as a model interaction site for further fundamental studies. For example, a cysteine mutant at this position could be created, and following crystallization in two dimensions, a disulfide bridge could be formed by oxidation of the adjacent side chains. This could be a means to stabilize the crystal form and to trap it in its kinetic state. Another possible mutation at this interaction site is leucine. It contains a hydrophobic side chain of the appropriate length for close packing and could be used to probe the importance of van der Waals and hydrophobic interactions in specific crystal contact regions.

Further work involving changes in environmental parameters is another avenue of investigation. For example, the study of temperature changes on 2D crystal growth would give further insight into the kinetic and thermodynamic parameters governing crystal growth. Alterations in subphase properties, such as salt concentration, could be a means to investigate interaction strength. Changes in solvent composition of the subphase could probe the contributions of different types of interactions, such as hydrophobic or van der Waals interaction, to crystallization.

One limitation of experimental approaches such as site-directed mutagenesis is their time- and labor-intensive nature. Therefore, it would be advantageous to develop an accurate computational model for predicting the lattice arrangement, thermodynamic properties, and kinetic properties of protein crystals containing mutated protein molecules. Völkel and Noolandi have developed a model which can computationally perform mutations in a straightforward manner and have applied it to predict protein−protein interactions and oligomer stability in the tumor suppressor p53.[88,89] In the model, protein structures and interactions are coarse-grained and a continuum approach is applied to describe the solvent as a continuous fluid.[90] While good qualitative agreement with experimental data has been obtained, certain environmental parameters (such as pH) are not easily addressed, and additional refinements of the model are currently in progress.

The issue of controlling molecular arrangement in protein arrays can conceivably be addressed with a combination of genetic methods, environmental changes, and computational modeling. At the initial stage, one would desire to form known crystals (such as *P*1, *P*2, or *C*222) at any given condition. This involves favoring interactions which are key for the formation of the desired crystal while disfavoring those in the growth of the undesired crystals. The eventual objective is the ability to specify any protein arrangement (not only the known "natural" crystal forms) to obtain desired crystal properties, which would be advantageous for the development of applications involving ordered proteins at surfaces.

Acknowledgment. We thank Tamara Coussaert, Sammy Farah, and Pasut Ratanabanangkoon for their gracious assistance with figures and the final version of this document. Patrick Stayton and Todd Edwards generously provided the wild-type streptavidin genes and the expression protocol. Wray Huestis, Chaitan Khosla, Roger Kornberg, and their group members are also gratefully acknowledged for allowing us use of their laboratory facilities. This work was funded by a Whitaker Foundation Graduate Fellowship and a William K. Bowes Fellowship to S.W.W., and NSF Grant BES-9729950 to A.P.G. and C.R.R.

References and Notes

(1) Gast, A. P.; Russel, W. B. *Phys. Today* **1998**, *51*, 24−30.
(2) Russel, W. B.; Saville, D. A.; Schowalter, W. R. *Colloidal Dispersions*; Cambridge University Press: Cambridge, 1989.
(3) Möhwald, H. *Annu. Rev. Phys. Chem.* **1990**, *41*, 441−476.
(4) McConnell, H. M. *Annu. Rev. Phys. Chem.* **1991**, *42*, 171−195.
(5) Jap, B. K.; Zulauf, M.; Scheybani, T.; Hefti, A.; Baumeister, W.; Aebi, U.; Engel, A. *Ultramicroscopy* **1992**, *46*, 45−84.
(6) Kornberg, R. D.; Darst, S. A. *Curr. Opin. Struct. Biol.* **1991**, *1*, 642−646.
(7) Olson, G. B.; Hartman, H. *J. Phys.* **1982**, *43*, 855−865.
(8) Lipp, M. M.; Lee, K. Y. C.; Zasadzinski, J. A.; Waring, A. J. *Science* **1996**, *273*, 1196−1199.

(9) Longo, M. L.; Bisagno, A. M.; Zasadzinski, J. A. N.; Bruni, R.; Waring, A. J. *Science* **1993**, *261*, 453−456.
(10) Sleytr, U. B.; Sara, M.; Messner, P.; Pum, D. *J. Cell. Biochem.* **1994**, *33*, 171−176.
(11) Kupcu, S.; Sleytr, U. B.; Sara, M. *J. Immunol. Methods* **1996**, *196*, 73−84.
(12) Hemming, S. A.; Bochkarev, A.; Darst, S. A.; Kornberg, R. D.; Ala, P.; Yang, D. S. C.; Edwards, A. M. *J. Mol. Biol.* **1995**, *246*, 308−316.
(13) Darst, S. A.; Edwards, A. M. *Curr. Opin. Struct. Biol.* **1995**, *5*, 640−644.
(14) Mosbach, K. *Immobilized Enzymes*; Academic Press: New York, 1976; Vol. 54.
(15) Blankenburg, R.; Meller, P.; Ringsdorf, H.; Salesse, C. *Biochemistry* **1989**, *28*, 8214−8221.
(16) Darst, S. A.; Ahlers, M.; Meller, P. H.; Kubalek, E. W.; Blankenburg, R.; Ribi, H. O.; Ringsdorf, H.; Kornberg, R. D. *Biophys. J.* **1991**, *59*, 387−396.
(17) Ku, A. C.; Darst, S. A.; Kornberg, R. D.; Robertson, C. R.; Gast, A. P. *Langmuir* **1992**, *8*, 2357−2360.
(18) Nelson, D. R.; Halperin, B. I. *Phys. Rev. B* **1979**, *19*, 2457−2484.
(19) Kosterlitz, J. M.; Thouless, D. J. *J. Phys. C.: Solid State Phys.* **1973**, *6*, 1181−1209.
(20) Strandburg, K. J. *Rev. Mod. Phys.* **1988**, *60*, 161−207.
(21) Young, A. P. *Phys. Rev. B* **1979**, *19*, 1855−1866.
(22) Bowden, N.; Terfort, A.; Carbeck, J.; Whitesides, G. M. *Science* **1997**, *276*, 233−235.
(23) Murray, C. A.; Sprenger, W. O.; Wenk, R. A. *Phys. Rev. B* **1990**, *42*, 688−703.
(24) Murray, C. A.; Vanwinkle, D. H.; Wenk, R. A. *Phase Transitions* **1990**, *21*, 93−126.
(25) Marcus, A. H.; Rice, S. A. *Phys. Rev. E* **1997**, *55*, 637−656.
(26) Knobler, C. M. *Science* **1990**, *249*, 870−874.
(27) Uzgiris, E. E.; Kornberg, R. D. *Nature* **1983**, *301*, 125−129.
(28) Ribi, H. O.; Ludwig, D. S.; Mercer, K. L.; Schoolnik, G. K.; Kornberg, R. D. *Science* **1988**, *239*, 1272−1276.
(29) Polyakov, A.; Severinova, E.; Darst, S. A. *Cell* **1995**, *83*, 365−373.
(30) Darst, S. A.; Ribi, H. O.; Pierce, D. W.; Kornberg, R. D. *J. Mol. Biol.* **1988**, *203*, 269−273.
(31) Frey, W.; Schief, W. R.; Pack, D. W.; Chen, C.-T.; Chilkoti, A.; Stayton, P.; Vogel, V.; Arnold, F. H. *Proc. Natl. Acad. Sci. U.S.A.* **1996**, *93*, 4937−4941.
(32) Leuther, K. K.; Bushnell, D. A.; Kornberg, R. D. *Cell* **1996**, *85*, 773−779.
(33) Asturias, F. J.; Meredith, G. D.; Poglitsch, C. L.; Kornberg, R. D. *J. Mol. Biol.* **1997**, *272*, 536−540.
(34) Amos, L. A.; Henderson, R.; Unwin, P. N. T. *Prog. Biophys. Mol. Biol.* **1982**, *39*, 183−231.
(35) Chaiet, L.; Wolf, F. J. *Arch. Biochem. Biophys.* **1964**, *106*, 1−5.
(36) Bayer, E. A.; Wilcheck, M. *Avidin−Biotin Technology*; Academic Press: San Diego, 1990; Vol. 184.
(37) Green, N. M. *Biochem. J.* **1966**, *101*, 774−780.
(38) Green, N. M. *Adv. Protein Chem.* **1975**, *29*, 85−133.
(39) Green, N. M. *Methods Enzymol.* **1990**, *184*, 51−67.
(40) Bayer, E. A.; Ben-Hur, H.; Wilcheck, M. *Methods Enzymol.* **1990**, *184*, 80−89.
(41) Weber, P. C.; Ohlendorf, D. H.; Wendoloski, J. J.; Salemme, F. R. *Science* **1989**, *243*, 85−88.
(42) Kraulis, P. J. J. *Appl. Crystallogr.* **1991**, *24*, 946−950.
(43) Hofmann, K.; Wood, S. W.; Brinton, C. C.; Montibeller, J. A.; Finn, F. M. *Proc. Natl. Acad. Sci. U.S.A.* **1980**, *77*, 4666−4668.
(44) Snejdárková, M.; Rehák, M.; Otto, M. *Anal. Chem.* **1993**, *65*, 665−668.
(45) Ebersole, R. C.; Miller, J. A.; Moran, J. R.; Ward, M. D. *J. Am. Chem. Soc.* **1990**, *112*, 2, 3239−3241.
(46) Müller, W.; Ringsdorf, H.; Rump, E.; Wildburg, G.; Zhang, X.; Angermaier, L.; Knoll, W.; Liley, M.; Spinke, J. *Science* **1993**, *262*, 1706−1708.
(47) Koppenol, S.; Stayton, P. S. *J. Pharm. Sci.* **1997**, *86*, 1204−1209.
(48) Freitag, S.; Trong, I. L.; Klumb, L.; Stayton, P.; Stenkamp, R. *Protein Sci.* **1997**, *6*, 1157−1166.
(49) Calvert, T. L.; Leckband, D. *Langmuir* **1997**, *13*, 6737−6745.
(50) Ku, A. C.-T. *The Growth of Two-Dimensional Streptavidin Crystals*; Stanford University: Stanford, 1996; p 98.
(51) Mullins, W. W.; Sekerka, R. F. *J. Appl. Phys.* **1963**, *34*, 323−329.
(52) Yatcilla, M. T.; Robertson, C. R.; Gast, A. P. *Langmuir* **1998**, *14*, 497−503.
(53) Ku, A. C.; Darst, S. A.; Kornberg, R. D.; Robertson, C. R.; Gast, A. P. *J. Phys. Chem.* **1993**, *97*, 3013−3016.
(54) Yatcilla, M. T. *Influence of pH on Two-Dimensional Crystals of Streptavidin*; Stanford University: Stanford, 1998; p 147.
(55) Vogel, V.; William R. Schief, J.; Frey, W. *Supramol. Sci.* **1997**, *4*, 163−171.
(56) Gallagher, W. H.; Croker, K. M. *Protein Sci.* **1994**, *3*, 1602−1604.
(57) Ataka, M.; Tanaka, S. *J. Phys. Soc. Jpn.* **1978**, *45*, 1779−1780.
(58) Wang, S.-W.; Poglitsch, C. L.; Yatcilla, M. T.; Robertson, C. R.; Gast, A. P. *Langmuir* **1997**, *13*, 5794−5798.
(59) Misell, D. L.; Brown, E. B. *Electron Diffraction: An Introduction for Biologists*; Elsevier: Amsterdam, 1987; Vol. 12.
(60) Wang, S.-W.; Robertson, C. R.; Gast, A. P. *Langmuir* **1999**, *15*, 1541−1548.
(61) Boodhoo, A.; Duke, N. E. C.; Kong, D.; Ritzel, M. W. L.; Kunimoto, D. Y.; Read, R. J. *J. Mol. Biol.* **1994**, *241*, 269−272.
(62) Lawson, D. M.; Artymiuk, P. J.; Yewdall, S. J.; Smith, J. M. A.; Livingstone, J. C.; Treffry, A.; Luzzago, A.; Levi, S.; Arosio, P.; Cesareni, G.; Thomas, C. D.; Shaw, W. V.; Harrison, P. M. *Nature* **1991**, *349*, 541−544.
(63) Braig, K.; Otwinowski, Z.; Hegde, R.; Boisvert, D. C.; Joachimiak, A.; Horwich, A. L.; Sigler, P. B. *Nature* **1994**, *371*, 578−586.
(64) Vijay-Kumar, S.; Senadhi, S. E.; Ealick, S. E.; Nagabhushan, T. L.; Trotta, P. P.; Kosecki, R.; Reichert, P.; Bugg, C. E. *J. Biol. Chem.* **1987**, *262*, 4804−4805.
(65) Takeda, S.; Yoshimura, H.; Endo, S.; Takahashi, T.; Nagayama, K. *Proteins: Struct., Funct., Genet.* **1995**, *23*, 548−556.
(66) Edwards, T. C.; Koppenol, S.; Frey, W.; Schief, W. R.; Vogel, V.; Stenkamp, R. E.; Stayton, P. S. *Langmuir* **1998**, *14*, 4683−4687.
(67) Wang, S.-W.; Robertson, C.; Gast, A.; Koppenol, S.; Edwards, T.; Vogel, V.; Stayton, P. 1999. In preparation.
(68) Chilkoti, A.; Tan, P. H.; Stayton, P. S. *Proc. Natl. Acad. Sci. U.S.A.* **1995**, *92*, 1754−1758.
(69) Argarana, C. E.; Kuntz, I. D.; Birken, S.; Axel, R.; Cantor, C. R. *Nucleic Acid Res.* **1986**, *14*, 1871−1882.
(70) Pahler, A.; Hendrickson, W. A.; Kolks, M. A.; Argarana, C. E.; Cantor, C. R. *J. Biol. Chem.* **1987**, *262*, 13933−13937.
(71) Wang, S.-W. *Effects of Interaction Modifications in Two-Dimensional Streptavidin Crystallization*; Stanford University: Stanford, 1999; p 114.
(72) Wilbur, D. S.; Stayton, P. S.; To, R.; Buhler, K. R.; Klumb, L. A.; Hamlin, D. K.; Stray, J. E.; Vessella, R. L. *Bioconjugate Chem.* **1998**, *9*, 100−107.
(73) Nargessi, R. D.; Smith, D. S. *Methods Enzymol.* **1986**, *122*, 67−72.
(74) Bruch, R. C.; Harold B. White, I. *Biochemistry* **1982**, *21*, 5334−5341.
(75) Bozzola, J. J.; Russell, L. D. *Electron Microscopy*; Jones and Bartlett Publishers: Boston, MA, 1992.
(76) Stewart, M. *J. Electron Microsc. Technol.* **1988**, *9*, 301−324.
(77) Creighton, T. E. *Proteins*; W. H. Freeman and Company: New York, 1993.
(78) Hindeleh, A. M.; Hosemann, R. *J. Mater. Sci.* **1991**, *26*, 5127−5133.
(79) Hosemann, R.; Hindeleh, A. M. *J. Macromol. Sci. Phys.* **1995**, *B34*, 327−356.
(80) Gabriel, B. L.; Taylor, K.; Creutz, C. E.; Kretsinger, R. H. *J. Struct. Biol.* **1991**, *107*, 29−37.
(81) Ewing, F. L.; Forsythe, E. L.; Woerd, M. v. d.; Pusey, M. L. *J. Cryst. Growth* **1996**, *160*, 389−397.
(82) Beckmann, W.; Otto, W. H. *Chem. Eng. Res. Des.* **1996**, *74*, 750−758.
(83) Tanaka, S.; Yamamoto, M.; Kawashima, K.; Ito, K.; Hayakawa, R.; Ataka, M. *J. Cryst. Growth* **1996**, *168*, 44−49.
(84) Tanaka, S.; Yamamoto, M.; Kawashima, K.; Ito, K.; Hayakawa, R.; Ataka, M. *Phys. Rev. E* **1997**, *56*, 67−69.
(85) Avrami, M. *J. Chem. Phys.* **1939**, *7*, 1103−1112.
(86) Bamford, C. H.; Tipper, C. F. H. *Reactions in the Solid State*; Elsevier Scientific Publishing Company: Amsterdam, 1980; Vol. 22.
(87) Cardew, P. T.; Davey, R. J. *Proc. R. Soc. London A* **1985**, *398*, 415−428.
(88) Völkel, A.; Noolandi, J. *J. Comput.-Aided Mater. Des.* **1996**, *3*, 289−295.
(89) Völkel, A.; Noolandi, J. *J. Comput.-Aided Mater. Des.* **1997**, *4*, 1−9.
(90) Skolnick, J.; Kolinski, A. *Science* **1990**, *250*, 1121−1124.